ELSEVIER

Journal of Power Sources 86 (2000) 523–530

JOURNAL OF POWER SOURCES

www.elsevier.com/locate/jpowsour

# Intrinsic reaction kinetics of methane steam reforming on a nickel/zirconia anode

A.L. Dicks, K.D. Pointon *, A. Siddle

*BG Technology, Ashby Road, Loughborough, Leicestershire, UK*

Accepted 18 October 1999

**Abstract**

For the purposes of optimising important system parameters in direct internally reforming (DIR) solid oxide fuel cell (SOFC) systems, a detailed knowledge of the methane steam reforming rate on the anode is needed. In order to shed light on the present poorly understood kinetics, a study of the methane steam reforming rate given by a typical thin electrolyte-supported nickel/zirconia SOFC anode has been carried out using a tubular plug flow differential reactor. These tests were essentially gradientless. The reaction rate was studied as a function of temperature (700–1000°C) and the partial pressure of methane (2–40 kPa), hydrogen (10–70 kPa) and steam (10–70 kPa). The total pressure was nominally 1 atm. The reaction was first order in methane with a weak positive effect of hydrogen, and a stronger negative effect of steam. The kinetics were complicated by the fact that reaction orders in hydrogen and steam were either temperature dependent and/or depended on the partial pressures of other components in the gas mixture. Furthermore, Arrhenius-type plots gave gradients which were dependent on the steam partial pressure. It is clear from this study that the reaction cannot be represented as simply as is generally attempted in the literature. An improved rate equation has been derived. 

*Keywords:* Solid oxide fuel cells; Nickel/zirconia anode; Steam-reforming; Reaction kinetics

## 1. Introduction

The existence of a widespread infrastructure for the supply of natural gas makes this an excellent fuel for the solid oxide fuel cell (SOFC). However, it must be first converted to a hydrogen-rich gas before its use in the SOFC. For methane, this involves the two reactions.

$$\text{Steam Reforming Reaction: } CH_4 + H_2O \rightarrow 3H_2 + CO \quad (1)$$

$$\text{Water} - \text{Gas Shift Reaction: } CO + H_2O \rightarrow H_2 + CO_2 \quad (2)$$

Similar reactions may be written for other hydrocarbons.

Industrial steam reforming is carried out over a nickel catalyst at elevated temperatures and the heat for the reaction is normally provided by direct firing. For fuel cell generators, external reformers have been developed which utilise heat generated in other parts of the system. This ensures that the overall system efficiency remains high. Various heat recovery techniques have been exploited.

The SOFC operates at a high enough temperature to allow the natural gas to be reformed within the fuel cell stack. This technique, called internal reforming, lowers the requirement for cell cooling and has many advantages relating to the capital cost and efficiency.

In the SOFC, the reforming of natural gas can be catalysed by the nickel/zirconia anode material, an approach known as direct internal reforming (DIR). However, natural gas usually contains significant quantities of higher hydrocarbons as well as methane. At the high temperatures of present SOFCs, these have a tendency to pyrolyse and produce unwanted materials such as carbon. This can degrade the performance of the anode and ultimately block the fuel channels. Therefore, it is envisaged that at least some external reforming of natural gas will be required in a real SOFC system to remove the higher hydrocarbons.

The modelling of internally reforming natural gas-fuelled SOFC systems requires an in-depth knowledge of the rate of methane steam reforming on nickel/zirconia anodes. Only with such a knowledge can important system

* Corresponding author. Tel.: +44-1509-283043; fax: +44-1509-283144; e-mail: kevin.pointon@bgtech.co.uk

0378-7753/00/$ - see front matter 
PII: S0378-7753(99)00447-4

parameters such as degree of internal/external reforming and anode recycle ratio be optimised to ensure acceptable temperature gradients, efficiency, etc.

A number of kinetic studies of the steam reforming of methane on nickel, nickel catalysts, and SOFC anodes are found in the literature and have been reviewed [1]. Unfortunately there is little agreement between the rate equations reported by different workers. Part of the problem can be traced to the almost universal assumption that the order of the reaction to product gas partial pressures is zero. This assumption comes from conventional wisdom of steam reforming catalysis, which bears little relevance to the SOFC where conditions of nickel particle size, support material, physical structure, gaseous composition, and temperature of operation, can all be significantly different from those employed industrially to steam reform methane.

In order to shed light on the kinetics, a study of the methane steam reforming rate given by a typical thin electrolyte-supported nickel/zirconia SOFC anode has been carried out using a tubular plug flow differential reactor.

## 2. Experimental

### 2.1. Sample preparation

The anode was a 40–60 μm screen-printed layer (55% Ni, porosity 40–45%) on a 150 μm-thick 5 × 5 cm YSZ plate. The BET surface area of the material, determined by nitrogen physical adsorption at 77 K, was 9.3 $m^2/g$. The active nickel surface area, determined by hydrogen chemisorption followed by temperature-programmed desorption, was 1.9 $m^2/g$.

To prepare the sample for the tubular reactor experiment, the anode was broken into pieces a few millimeters in size which were set into an alumina boat of semi-circular cross-section and length about 14 cm. This construction was of the correct size to fit snugly into the stainless steel tubular microreactor (9.5 mm o.d., 6.5 mm i.d.). The material of the reactor was verified as practically inactive towards steam reforming by carrying out experiments with no anode present.

The tube was located in a furnace and the boat was held in place in the tube, against the flow of reactant gas, by the furnace control thermocouple which was also set into the boat and held in contact with a central piece of anode. The complete assembly is shown in Fig. 1.

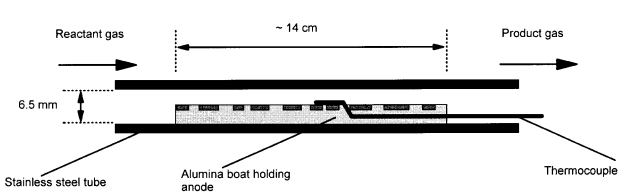


Fig. 1. Cross-section of tubular micro-reactor.

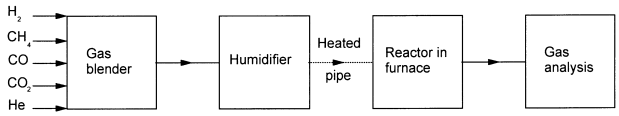


Fig. 2. Block diagram of the experimental rig for kinetic experiments.

### 2.2. Experimental rig

The experimental rig consisted of a gas blender, a humidifier, a furnace and gas analysis equipment as shown in Fig. 2. The gas blender was capable of delivering up to five dry gases from air, nitrogen, argon, methane, carbon monoxide, carbon dioxide and hydrogen. The flow rates were controlled by mass flow controllers and are expressed at standard conditions of 0°C and 1 atm throughout this report. A two-stage humidifier was used to add steam by bubbling the dry gas through water at an appropriate temperature. The furnace contained the reactor and was capable of controlling the temperature of the reactor up to 1000°C with the control thermocouple in close contact with the test piece. All pipes and valves between the humidifier and furnace were heated to prevent condensation of steam. Downstream of the furnace, gas analysis was performed with an Ai Cambridge Gas Chromatograph (after dehumidification by cooling).

### 2.3. Test procedure

The sample was heated to 950°C whereupon the anode was reduced in a 500 ml/min hydrogen/argon mixture. The hydrogen concentration was gradually increased from 0.125% to 100% over a period of 3 h in a series of timed step changes. The temperature was then ramped to the test temperature at 20°C/min and steam reforming was initiated. Changes to the individual gas partial pressures experienced by the sample were always carried out strictly in an appropriate order to prevent carbon deposition.

The total flowrate was maintained in the range 750–1600 ml/min in order to keep the methane conversion achieved by the sample to around 10% or less. Thus, gaseous compositions were approximately constant over the length of the sample and the reactor behaved in an approximately differential manner. Furthermore, the reaction rate was independent of flowrate over a relatively wide range (see Fig. 3) and in gas mixtures diluted with argon or helium, the nature of the diluent (which affects binary diffusion coefficients by a factor of 3) did not greatly affect the reforming rate (around 4%). These facts indicate that mass transfer effects were unimportant. The experiments were, therefore, essentially gradientless and measured intrinsic kinetics.

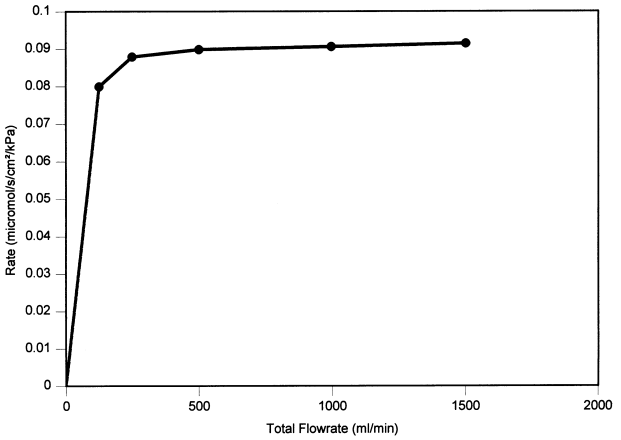


Fig. 3. Reforming rate vs. flowrate in the microreactor (7 kPa methane, 30 kPa steam, 30 kPa hydrogen, 850°C).

The reactor was operated at a nominal pressure of 1 atm. Most measurements were made in the temperature range 800–900°C. However, a small number of experiments were carried out in the temperature range 700–1000°C in order to obtain a more complete picture of the temperature-dependence of the reaction.

The reactor offered no means of applying an oxygen ion flux. The measurements were, therefore, made as if under open circuit conditions. Whilst a real SOFC system would be producing current and this could quite possibly influence the reforming rate through 'non-faradaic electrochemical modification of catalyst activity' effects [2], it is important to fully understand the reaction kinetics under open circuit conditions before considering the effect of current flow.

For each gas composition, gas chromatography (GC) analysis was carried out on the outlet and inlet gas streams after 2 h equilibration time. These analyses could be used to calculate the rate of reforming from the difference in composition between inlet and outlet streams.

Individual experiments required up to several months to complete. It was recognised that the activity of the sample might change during that period. Therefore, a standard gas composition was chosen and the sample was tested with this composition at the start of each day. All the measured rates on that day could then be scaled accordingly in order to put them on the same basis as those measured on the first day.

### 2.4. Test programme

The experimental set-up described above is not well suited to measuring the rate of steam reforming under reactant conditions far from shift equilibrium. This is because the shift reaction is recognised as being very rapid, leading to possible concentration gradients. Furthermore, by the time a small portion of the reforming has occurred, most of the shift reaction has already occurred, and the reactor is no longer a differential one.

The practical result of these considerations is that, although it was assumed that all components in the gas mixture could affect the rate, the effect of the individual partial pressures present cannot all be studied independently. Instead, mixtures of hydrogen, methane and steam were studied eliminating the possibility of shift reaction amongst the inlet gases. A matrix of compositions was tested as shown below.

10 kPa $< P_{H_2} <$ 70 kPa,
10 kPa $< P_{H_2O} <$ 70 kPa,
2 kPa $< P_{CH_4} <$ 40 kPa,
balance helium,

where $P_X$ is the partial pressure of gas $X$.

In all cases, the compositions utilised were not influenced by carbon deposition on thermodynamic grounds over the temperature range of the tests (800–900°C).

## 3. Results and discussion

### 3.1. The effect of temperature

Fig. 4 shows an Arrhenius-type plot for 30% $H_2$/8% $CH_4$ gas mixtures with various steam contents over the temperature range 700–1000°C. The reaction rate plotted in this diagram and in all subsequent ones is defined as

$$\text{rate} = -\mathrm{d}N_{CH_4}/\mathrm{d}t \quad (3)$$

i.e., the rate of consumption of moles of methane per/unit of geometric area of anode ($N_{CH_4}$) with time ($t$). It is valid to plot rate in this diagram rather than rate constant because the gas compositions did not vary greatly with temperature.

Clearly the plots shown in Fig. 4 are not linear, the local gradients implying activation energies of 118–294 kJ/mol. Furthermore, the local gradients appear to be a function of gas composition as well as temperature.

Similar trends were obtained for the many gas compositions studied in the temperature range 800–900°C. An

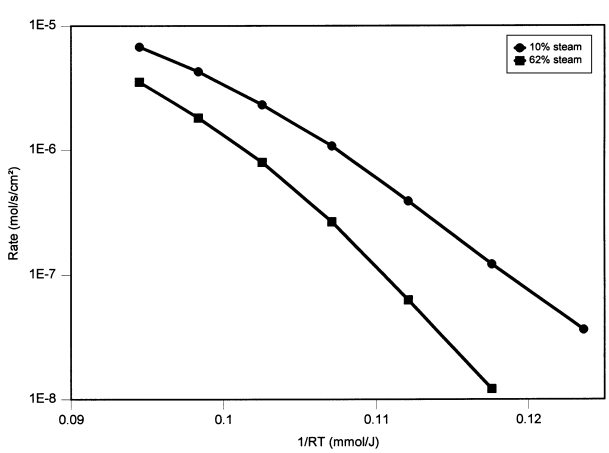


Fig. 4. Arrhenius plots for mixtures of 8%, methane, 30% hydrogen, various steam, balance helium.

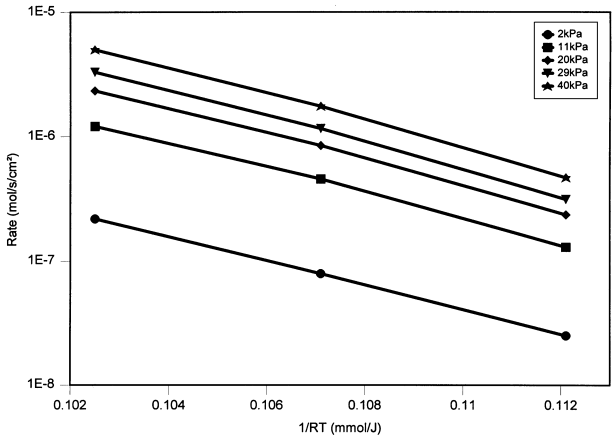


Fig. 5. Arrhenius plots for mixtures of 50 kPa steam, 10 kPa hydrogen, various methane partial pressures.

example of the results obtained is given in Fig. 5 and shows wholly typical trends. The mean gradients in the temperature range of interest were 154–253 kJ/mol, depending on the gas composition.

Fig. 6 indicates the manner in which the mean gradients of Arrhenius plots in the range 800–900°C varied with composition. Clearly the partial pressures of methane and hydrogen are relatively unimportant, but the partial pressure of steam has a significant effect.

The non-linearity and composition-dependence of the Arrhenius plots may partly explain why the literature values observed for the activation energy of the steam-reforming reaction on SOFC anodes varies so significantly. The literature values were reviewed by Pointon [1] and vary between 35 and 287 kJ/mol. A portion of this variation may simply be due to the fact that different workers have used different gas compositions.

### 3.2. The effect of the gas composition

The dependence of rate on methane partial pressure is shown in Fig. 7 which refers to 50 kPa $H_2$/30 kPa $H_2O$ mixtures. Similar diagrams for all other steam and hydrogen partial pressures revealed identical trends and are not therefore given in this report. The order of the reaction with respect to methane was always close to 1 regardless of the temperature and partial pressures of steam and hydrogen.

The reaction rate was found to be a function of the hydrogen partial pressure as shown for 850°C in Fig. 8. In this figure, the influence of methane partial pressure has been eliminated by plotting rate divided by methane partial pressure, a technique which is valid because the reaction order is generally 1 for methane. Fig. 8 reveals a relatively

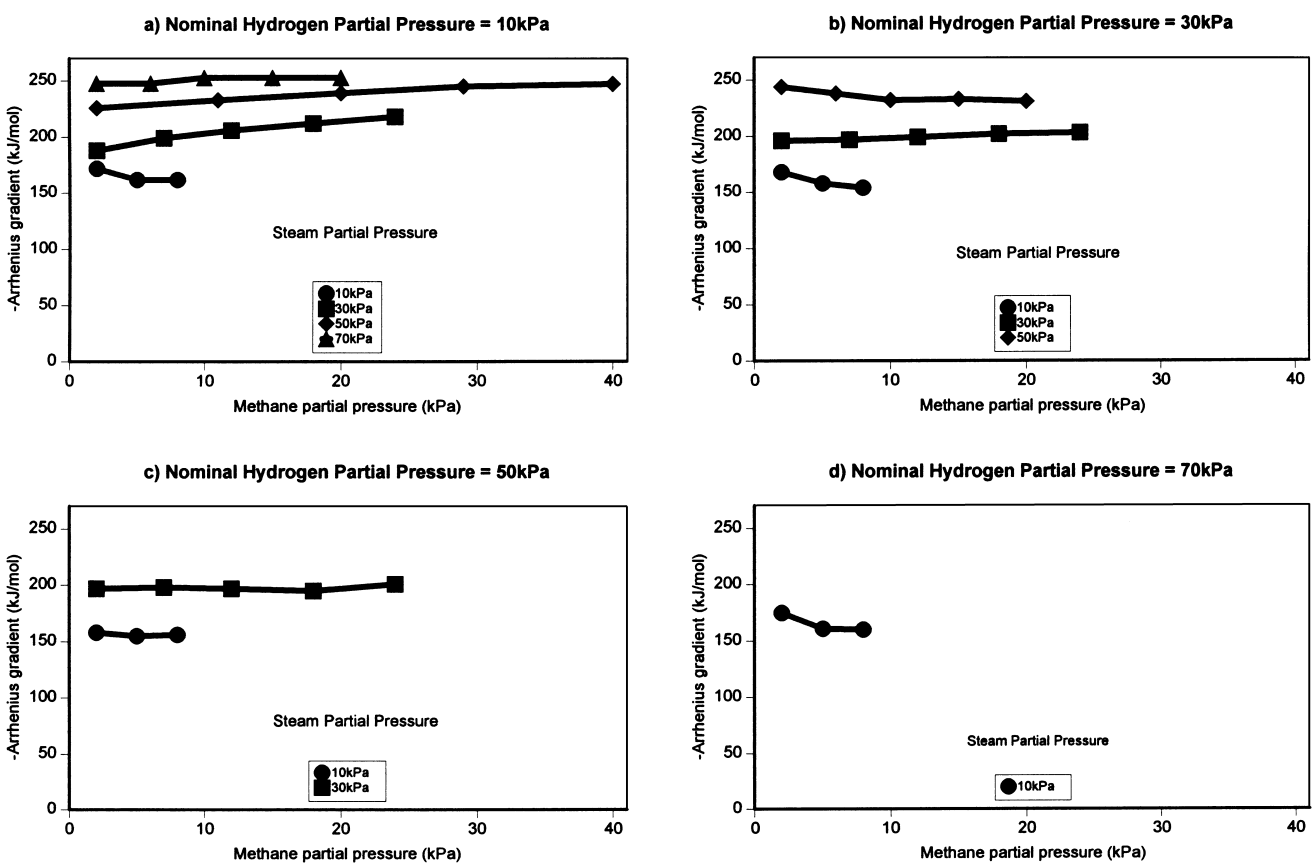


Fig. 6. Effect of gas composition on the temperature dependence of steam reforming rate.

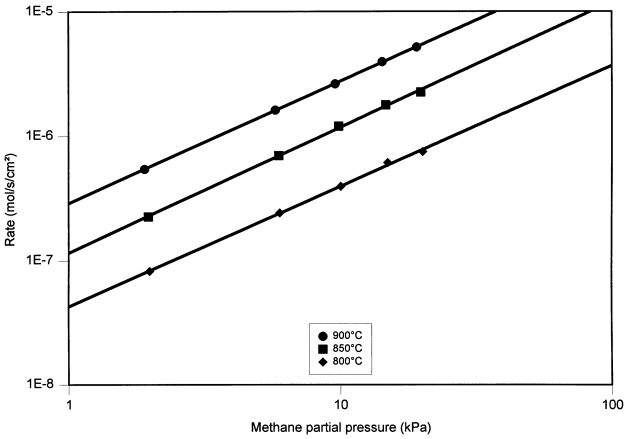


Fig. 7. Influence of methane partial pressure on reforming rate (30 kPa steam, 50 kPa hydrogen).

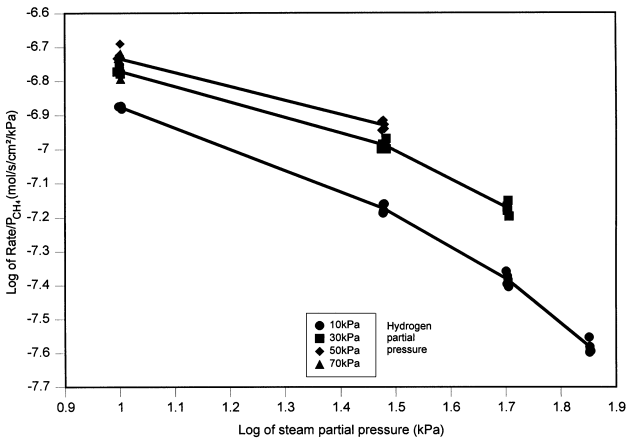


Fig. 9. Influence of steam partial pressure on reforming rate at 850°C.

weak positive effect of hydrogen on the rate which becomes slightly stronger with increasing steam partial pressure (the figure implies reaction orders of 0.23–0.45 when 10 kPa $< P_{H_2} <$ 30 kPa). These trends were independent of temperature in the range 800–900°C.

A significant effect on rate due to steam was observed. Fig. 9 gives the variation of rate due to steam partial pressure at 850°C. A strong negative effect is apparent. Close inspection of the figure reveals that the effect of steam depends on hydrogen partial pressure (the apparent reaction order with respect to steam was between $-0.63$ and $-0.41$ at 850°C when 10 kPa $< P_{H_2O} <$ 30 kPa). However, unlike the effect of hydrogen partial pressure, the effect of steam partial pressure depended on temperature (see Fig. 10). For example, as Fig. 10 shows, the mean reaction order for steam over the range 10 kPa $< P_{H_2O} <$ 70 kPa varied from $-0.4$ at 900°C to $-0.82$ at 800°C when the $H_2$ partial pressure was 10 kPa.

The existence of mass transfer effects has been invoked in the literature [3] to explain the steam-dependence of methane reforming by nickel/zirconia. As mentioned above, a strong influence of steam partial pressure is evident in our study. However, in our study, concentration gradients did not appear to be present. This fact is revealed by helium and argon dilution experiments which resulted in the same rate irrespective of the nature of the diluent even though binary diffusion coefficients are larger in helium than in argon by a factor of 3. A large gaseous hourly space velocity was chosen to inhibit the formation of a boundary layer but mass transfer effects were possible within the porous anode. The apparent absence of these mass transfer effects may have been a result of the thinness of the anode and its specific porous properties.

### 3.3. Reaction mechanism

Whilst none of the work described in this paper has been aimed specifically at identifying the reaction mechanism on nickel/zirconia (for example, by identifying reaction intermediates), the qualitative trends highlighted above shed some light on the mechanism. This is because the measured rates apparently reflect intrinsic kinetics (mass transfer effects are absent) and, therefore, are a consequence of this mechanism alone.

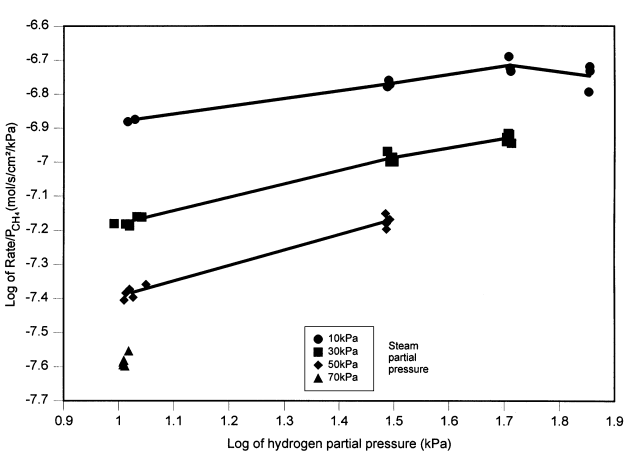


Fig. 8. Influence of hydrogen partial pressure on reforming rate at 850°C.

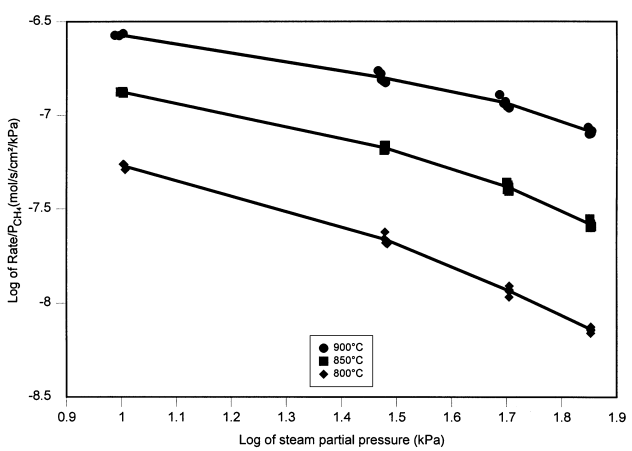


Fig. 10. Effect of temperature on the influence of steam partial pressure (10 kPa hydrogen).

The first-order dependence of the rate on methane partial pressure is a recurring theme in the literature and is consistent with the most generally-accepted rate-determining step for the reaction, namely methane chemisorption. Nevertheless, the Arrhenius gradients described above differ significantly from the activation energy for deuterium exchange in methane over nickel (100–135 kJ/mol [4] depending on how many hydrogen atoms are replaced).

This fact, together with the non-linearity and composition-dependence of the Arrhenius plots, is perhaps not surprising if a mechanism of the type described by Boudart [5] and others, e.g. Ref. [6], is pertained. Of these types, the most appropriate to the ternary mixtures is as follows:

$$CH_4 + n^* \rightarrow CH_x - {}^*n + (4-x)/2H_2 \quad (4)$$

$$H_2O + {}^* \rightleftarrows O - {}^* + H_2 \quad (5)$$

$$CH_x - {}^*n + O - {}^* \rightarrow CO + x/2H_2 + (n+1)^* \quad (6)$$

$$H_2 + 2^* \rightleftarrows 2H - {}^* \quad (7)$$

where * represents an active surface site. In this type of mechanism, slow methane adsorption (reaction 4) and rapid steam adsorption (reaction 5) give rise to surface carbon-containing species and surface oxygen or hydroxyl species. Rapid reaction between these species results in product CO (reaction 6). Hydrogen is assumed to be adsorbed at equilibrium levels (reaction 7).

The existence of a dependence of the rate on product partial pressure as well as reactant partial pressure is a possibility which is largely ignored in the SOFC literature. However, the effect is unsurprising in the light of reaction mechanisms such as those described above, because product gas chemisorption may interfere with methane chemisorption by occupying active surface sites. Effects such as these may largely account for the disagreement in the literature concerning the rate equation, because experimentalists have not always controlled the gas composition closely enough.

### 3.4. Rate equation

Assuming Langmuir adsorption isotherms, the kinetics resulting from the above mechanism involve a rate, the temperature-dependence of which is determined by a pair of temperature-dependent equilibrium constants, and not simply activation of the rate-determining step.

$$\text{rate} = \frac{k(T)\,P_{CH_4}}{\left(1 + K_H(T)\,P_{H_2}^{1/2} + K_S(T)\,P_{H_2O}/P_{H_2}\right)^n} \quad (8)$$

where $k(T)$ is the rate constant, $P_X$ is the partial pressure of gas $X$, $K_H(T)$ is the equilibrium constant for hydrogen adsorption, $K_S(T)$ is the equilibrium constant for steam adsorption and $n$ is the number of surface sites required for methane adsorption.

This rate equation can accommodate all of the experimental observations described above. Non-Arrhenius behaviour is a consequence of the existence of temperature-dependent equilibrium constants in the equation. The apparent activation energies are expected to be composition-dependent because of the terms in $P_{H_2}$ and $P_{H_2O}$ in the denominator.

A negative hydrogen-dependent effect of steam is a consequence of the presence of the $P_{H_2O}/P_{H_2}$ term in the denominator; it is temperature-dependent since the term is multiplied by a temperature-dependent constant. A positive steam-dependent effect of hydrogen is a consequence of the same terms, temperature independence being possible by fortuitous balancing of the $K_H(T)P_{H_2}$ term over the limited temperature range studied.

For the purposes of fitting the data to this equation, $K_H(T)$ and $K_S(T)$ were allowed to vary linearly with the absolute temperature ($T$).

$$K_H(T) = K_H^0 + K_H' T \quad (9)$$

$$K_S(T) = K_S^0 + K_S' T \quad (10)$$

The rate constant was described by the Arrhenius equation,

$$k(T) = k_0 \mathrm{EXP}(-E_a/RT) \quad (11)$$

where $R$ is the universal gas constant, $k_0$ is the frequency factor and $E_a$ is the activation energy for the rate-determining step.

When $n$ was taken as 1, a good fit to the data was possible only at unrealistic values of $E_a$ ($>250$ kJ/mol), and the equilibrium constants were then unphysical (negative). Taking $n=2$ resulted in a good fit over a wide range of $E_a$, spanning realistic values, and realistic equilibrium constants were also obtained. Consequently, $E_a$ was taken as the value for deuterium exchange in methane over nickel (135 kJ/mol). The value of $k_0$ then obtained was also realistic, being of the same order of magnitude as the collision frequency for methane molecules with surface nickel atoms (around 21 mol $s^{-1}$ $cm^{-2}$ $bar^{-1}$ at 800–900°C, given the active metal area, 1.9 $m^2/g$, and the approximate coating weight of the anode, 0.1 g/cell).

Fig. 11 summarises the fit of the experimental rates to the rate equation, and whilst there is some scatter, the fit is useful.

### 3.5. Implications of the rate equation

Eq. (8) implies that the reforming rate vanishes at zero hydrogen concentration. The physical explanation for this is that flooding of surface sites with rapidly adsorbed steam occurs because the absence of hydrogen pushes reaction 5 to completion. Experiments utilising purely steam/methane mixtures confirmed very low rates in the micro-reactor.

In practical terms, this observation highlights the importance of some pre-reforming, because steam:methane mixtures could give rise to a portion of the stack near the inlet

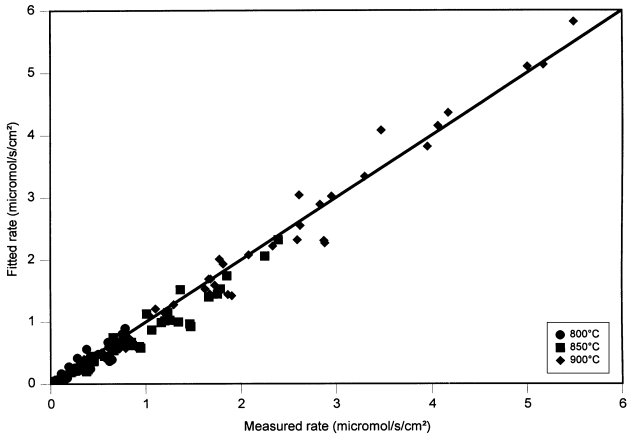


Fig. 11. Fit of rates obtained with ternary mixtures to a mechanism by Boudart.

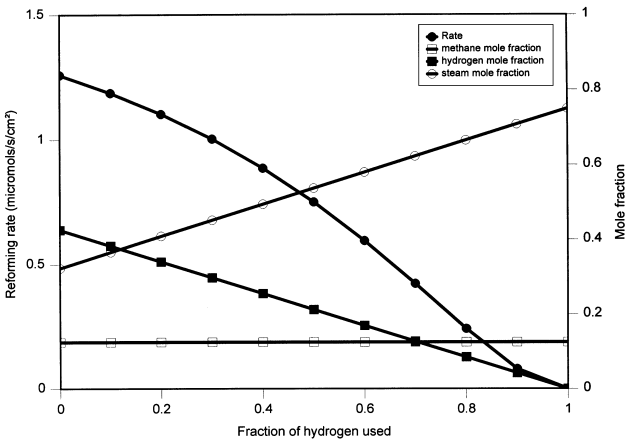


Fig. 13. Compositional changes due to hydrogen utilisation and effect on predicted rate (850°C, 1 bar, s/c = 2.0, 50% pre-reforming).

where there is no hydrogen fuel. This could arise because of the finite time required for the low initial reaction rate to build up sufficient hydrogen to support higher reaction rates.

A second implication of Eq. (8) is that there is a maximum in the reforming rate as the degree of pre-reforming increases. This is because, given the variation in gas composition together with the trends inherent in Eq. (8), the changing steam and hydrogen partial pressure affect the rate in the opposite sense to methane. The two competing effects result in a maximum. Fig. 12 gives the variation in gas composition as the degree of pre-reforming (fraction of methane reformed) increases, shift reaction being assumed to be at equilibrium at 850°C and 1 bar. The rates calculated by Eq. (8) from these compositions are also shown on the diagram. A maximum at about 30% pre-reforming is observed. Initial experimental measurements on full gas mixtures (at shift equilibrium) are consistent with this trend.

In Fig. 13, the effect on gas composition of oxidation of a fraction of the available hydrogen is given along with the reforming rates implied by Eq. (8). Here, as the amount of oxidation increases, hydrogen is replaced by an equivalent amount of steam, both effects tending to reduce the reforming rate. It is important to note that the often-quoted simple first order kinetics fails completely to predict this trend, since the methane partial pressure is constant (first order kinetics predicts constant reforming rates with increasing oxidation).

The overall effect of the initial steam:methane (s/c) ratio (when some pre-reforming is allowed for to give reaction-supporting hydrogen) is to reduce the reforming rate as s/c increases (Fig. 14).

The above observations suggest that the options for manipulating the compositions seen by the SOFC stack to obtained optimal reforming rates, temperature gradients and system efficiency via system configuration, anode recycle, etc., may be much greater than implied by the simple first order kinetics normally assumed.

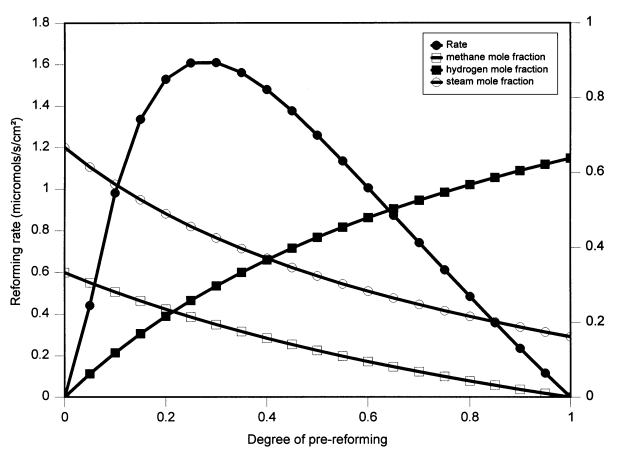


Fig. 12. Compositional changes due to pre-reforming and effect on predicted rate (850°C, 1 bar, s/c = 2.0).

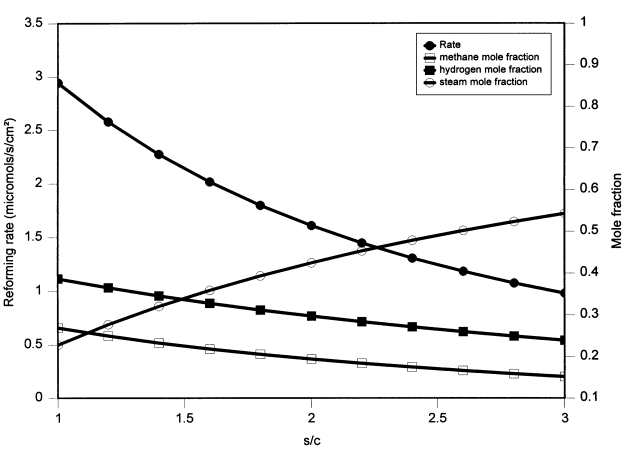


Fig. 14. Compositional changes due to initial s/c ratio and effect on predicted rate (850°C, 1 bar, 30% pre-reforming).

## 4. Conclusions

(1) The steam reforming of methane over the nickel/zirconia anode exhibits non-Arrhenius behaviour in the temperature range 700–1000°C. The dependence of rate on temperature is itself a function of both temperature and gas composition.

(2) The reaction is first order with methane which is consistent with rate-determining methane adsorption.

(3) A positive effect of the hydrogen partial pressure and a negative effect of the steam partial pressure on the rate of internal reforming is evident. The strength of the effect for either of these gases is dependent on the amount of the other gas present. However, whilst the effect of steam is dependent on temperature, that of hydrogen is not.

(4) The rate of steam reforming in purely methane/steam mixtures is low. Some hydrogen must be present to support significant reforming rates.

(5) These observations are all broadly consistent with rate-determining methane chemisorption, rapid surface reaction of methane-derived and oxygen-derived surface species, rapid desorption of product CO and rapid dissociative chemisorption of steam and hydrogen.

(6) Assuming Langmuir adsorption isotherms,

$$\text{rate of reforming reaction} = \frac{k(T)\,P_{\mathrm{CH_4}}}{\left(1 + K_{\mathrm{H}}(T)\,P_{\mathrm{H_2}}^{1/2} + K_{\mathrm{S}}(T)\,P_{\mathrm{H_2O}}/P_{\mathrm{H_2}}\right)^{n}}$$

where $k(T)$ is the rate constant, $P_X$ is the partial pressure of gas $X$, $K_{\mathrm{H}}(T)$ is the equilibrium constant for hydrogen adsorption, $K_{\mathrm{S}}(T)$ is the equilibrium constant for steam adsorption and $n$ is the number of surface sites required for methane adsorption.

(7) The above equation fits the experimental data well.

## Acknowledgements

We would like to acknowledge the financial support of the DTI through the Energy Technology Support Unit (ETSU) and the European Commission under the Joule III programme.

## References

[1] K.D. Pointon, Review of Work on Internal Reforming in the Solid Oxide Fuel Cell, ETSU report F/01/00121/REP, 1997.
[2] C.G. Vayenas, S. Bebelis, I.V. Yentekakis, H.-G. Lintz, Catalysis Today 11 (3) (1990) 303–442.
[3] E. Achenbach, E. Riensche, Journal of Power Sources 52 (1994) 283–288.
[4] C. Kemble, Catalysis Review 5 (1971) 33.
[5] M. Boudart, AIChE Journal 18 (1972) 465.
[6] N.M. Bodrov, L.O. Apel'baum, M.I. Tempkin, Kinetics and Catalysis 5 (4) (1964) 614–622.